Environmental application of the all-sky survey high-resolution air-shower (ASHRA) telescope — aerosol distribution measurement using a bistatic, imaging lidar

Shunsuke Fukagawa [a], Ikue Kouga [a, c], Hiroaki Kuze [a], Nobuo Takeuchi [a],
Makoto Sasaki [b], Yoichi Asaoka [b], Satoru Ogawa [c]

[a] *Center for Environmental Remote Sensing (CEReS), Chiba University*
1-33 Yayoi-chi, Inage-ku, Chiba 263-8522, Japan

[b] *Institute for Cosmic Ray Research, University of Tokyo*
5-1-5 Kashiwa-no-Ha, Kashiwa City, Chiba 277-8582, Japan

[c] *Faculty of Science, Toho University*
2-2-1 Miyama, Funabashi City, Chiba 274-8510, Japan

Abstract: All-sky Survey High Resolution Air-shower (Ashra) telescope has been developed to detect cosmic-ray neutrinos with extremely high energy, larger than 10^{16} eV. The important features of the telescope system are the wide FOV (50×50 deg) with high angular resolution (1 arcmin) and a high-speed, highly sensitive imaging system with an intelligent triggering capability. In this paper we report an imaging lidar on the basis of this novel telescope system applied to the detection of atmospheric aerosols. Because of the wide acceptance angel, the bistatic configuration enables light detection in the forward-scattering mode, greatly enhancing the signal-to-noise ratio. Eye-safe lidar operation is achieved with a laser wavelength in the operational wavelength range of the Ashra telescope (300-420 nm). Simulation studies are undertaken to establish the retrieval algorithm of aerosol distribution from the bistatic measurement.

1. Introduction

The All-sky Survey High Resolution Air-shower (Ashra) telescope project is a combined effort in the different categories of cosmic-ray physics, particle physics, and remote-sensing techniques of atmospheric sounding. In this project, the CEReS group is in charge of the application of the Ashra telescope to the monitoring of the atmosphere. The novel concept of Ashra telescope has been developed by the group of Institute for Cosmic Ray Research (ICRR), University of Tokyo. The remarkable features of the system are a wide field-of-view (FOV) (50 × 50 deg) with high angular resolution (1 arcmin = 0.29 μrad) and a high-speed, highly sensitive imaging system with an intelligent triggering capability [1-4].

The imaging lidar observation[5] is conducted in bistatic mode, in which, unlike the conventional monostatic lidar, the telescope is placed apart from the laser source. The light scattered in the atmosphere is detected in the scattering-angel range of $0<\theta<180$ deg. Although bistatic measurements of aerosols have so far been reported[6,7], the scanning of the laser beam was not attempted, leading mainly to the detection near the backscattering scheme. In contrast, forward scattering yields high signal-to-noise (S/N) ratio owing to the general property of the Mie scattering from aerosols. In the case of Ashra system, another advantage is the usage of the intelligent triggering. This greatly contributes to reduce the background light and thereby to increase the S/N ratio. These features make the three-dimensional, wide area, and real-time monitoring of atmospheric aerosols possible. Moreover, using the laser wavelength at 351nm

or 355 nm, which are in the design wavelength of Ashra telescope (300-420 nm), ensures eye-safe lidar operation, since the level of maximum permissible exposure (MPE) is very high in this wavelength region.

In this paper, we describe the scheme of bistatic lidar measurement, with the results of related simulations and our preliminary experiment of the bistatic lidar measurement.

2. Bistatic measurement of aerosol

The basic configuration of the bistatic measurement is shown in Fig. 1. A laser and a telescope are located separately, with a baseline distance of L. The laser is illuminating a direction θ_{laser} (elevation angle), while the telescope is observing the beam path toward a direction θ_{view}. In this bistatic measurement, the lidar equation is written as

$$P = P_0 \, K \frac{A}{r^2} \, ds \, \beta(\theta_{scat}) \, T \, , \tag{1}$$

where P is the received signal intensity, P_0 the emitted laser intensity, K the efficiency of the receiving optics, A the area of telescope's mirror, r the distance between the target (aerosol particle) and the telescope, and θ_{scat} the scattering angle. The portion of the laser beam path subtended by the FOV for a single pixel of the array detector is denoted as ds, which is given as

$$ds = \frac{r \, \theta_{FOV}}{\sin(\theta_{scat})} . \tag{2}$$

The generalized scattering coefficient, $\beta(\theta_{scat})$, is defined as

$$\beta(\theta_{scat}) = \alpha_1 \, f_1(\theta_{scat}) + \alpha_2 \, f_2(\theta_{scat}) \, . \tag{3}$$

Here, θ_{FOV} is the FOV for a single pixel, α the extinction coefficient, and f the phase function. Subscript 1 is for aerosol and 2 for air molecule. The transmittance along the combined laser path and viewing path is expressed as

$$T = \exp[-(\tau_t + \tau_r)] . \tag{4}$$

Here, τ_t is the optical thickness of the transmitter side and τ_r that of the receiver side. These parameter are given as

$$\tau_t = \frac{\int_0^z \{\alpha_1(z') + \alpha_2(z')\} dz'}{\sin\theta_{laser}} , \tag{5}$$

$$\tau_r = \frac{\int_0^z \{\alpha_1(z') + \alpha_2(z')\} dz'}{\sin\theta_{view}} . \tag{6}$$

3. Inversion of bistatic lidar data

In this section, we describe the inversion procedure used to derive the spatial distribution of the aerosol extinction coefficient from the bistatic lidar data. We assume that the laser beam is scanned as shown in Fig. 2. The viewing direction is numbered with an index i (= 0, 1, ...) and the laser beam direction with j (= 0, 1, ...). The aerosol extinction coefficient (i.e. the product of the aerosol number density and the total cross section) at the intersection defined by indices i and j is expressed as $\alpha_1^{(i,j)}$. From Eqs. (1) and (2), the ratio of the received signal intensities at (i, j) and $(i, j+1)$ is given as

$$\frac{P^{(i,j+1)}}{P^{(i,j)}} = \frac{\beta(\theta_{scat}^{(i,j+1)}) \, r^{(i,j)} \sin(\theta_{scat}^{(i,j)}) T^{(i,j+1)}}{\beta(\theta_{scat}^{(i,j)}) \, r^{(i,j+1)} \sin(\theta_{scat}^{(i,j+1)}) T^{(i,j)}} \tag{7}$$

If $\alpha_1^{(i,j)}$ is known, this equation can be used to calculate $\alpha_1^{(i,j+1)}$ from the bistatic lidar data. For this purpose, we define an error

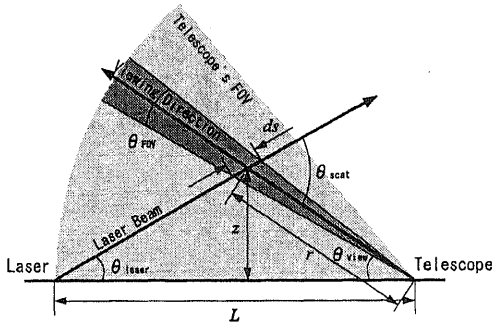

Fig.1 Schematic diagram of the bistatic measurement.

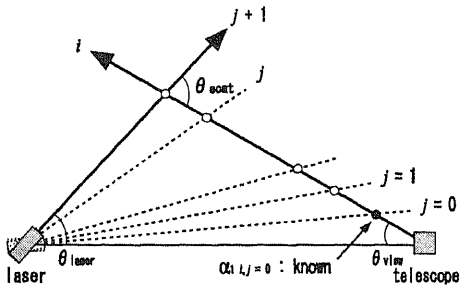

Fig.2 Schematic diagram of the inversion algorithm.

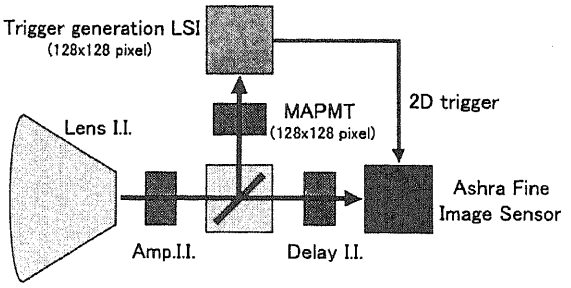

Fig.3 Schematic diagram of the imaging system of Ashra telescope with the intelligent trigger.

parameter ε as the difference between the calculated ratio and the observed ratio of the signal intensities:

$$\varepsilon = \frac{P_{\mathrm{obs}}^{(i,j+1)}}{P_{\mathrm{obs}}^{(i,j)}} - \frac{P^{(i,j+1)}}{P^{(i,j)}}. \quad (8)$$

Here, P_{obs} is the observed intensity and P is theoretically calculated using Eq.(1). The bisection method is employed to search the minimum value of $|\varepsilon|$ by changing $\alpha_1^{(i,j+1)}$. Since the boundary condition, $\alpha_1^{(i,0)}$, can be obtained from the ground-based scattering measurement, the sequential application of the present procedure yields all the required values of $\alpha_1^{(i,j)}$. In practice, the application has to be iterative, since the value of the transmission T in Eq.(4) is improved successively: values of the optical thickness in Eq.(4) are re-calculated using the equations of

$$\tau_{\mathrm{t}}^{(i,j)} = \sum_{n=0}^{i-1} \frac{\alpha_1^{(n+1,j)} + \alpha_1^{(n,j)}}{2} \frac{z^{(n+1,j)} - z^{(n,j)}}{\sin(\theta_{\mathrm{laser}}^{j})}, \quad (9)$$

$$\tau_{\mathrm{r}}^{(i,j)} = \sum_{n=0}^{j-1} \frac{\alpha_1^{(i,n+1)} + \alpha_1^{(i,n)}}{2} \frac{z^{(i,n+1)} - z^{(i,n)}}{\sin(\theta_{\mathrm{view}}^{i})}, \quad (10)$$

where z is the height of the intersection point. The iterative calculation is repeated until the extinction coefficient at each intersection point converges.

3. Simulation

3.1 Signal-to-Noise Ratio

The schematic diagram of the imaging system of Ashra telescope is shown in Fig. 3. The image signal that passes through an amplification image intensifier (Amp. I.I.) is split into two paths. The first path is toward a Delay I.I. before reaching a fine image sensor, and the other path is connected to a multi-anode photo multiplier tube (MAPMT, 128 × 128 pixels). If the signal intensity detected by a certain pixel on MAPMT exceeds a trigger level, only a pixel region on the fine image sensor that corresponds to the pixel position on MAPMT is gated. The temporal width of the gate is determined by the time period in which the MAPMT pixel detects the signal (> a few ns). This operation minimizes the accumulation of sky background light on the fine image sensor, hence the S/N ratio is expected to increase significantly.

The estimation of the S/N ratio is conducted for the bistatic lidar system with and without the intelligent trigger. An example of the calculated S/N ratio is shown in Fig. 4. This simulation is based on a spectrum of daytime sky radiance reported by C.P. Jacovides et.al[8] and the aerosol extinction coefficient at the ground level of 1.0×10^{-4} m^{-1}. The vertical profile is proportional to an extinction profile model reported by Sasano[9]. Figure 4 shows that the usage of the intelligent trigger enhances the S/N ratio by 2-3 orders of magnitude. A related advantage of the bistatic lidar measurement as compared with the monostatic case is the limited variation in the dynamic range of the signal intensity, which results in the ease in the detector design as a whole.

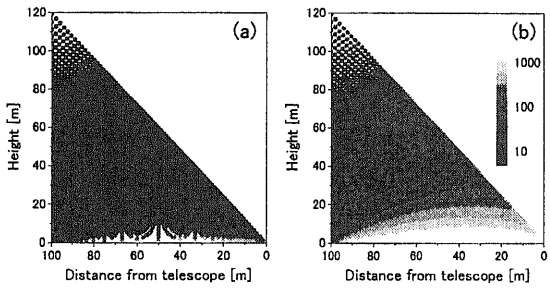

Fig.4 Two-dimensional distribution of the S/N ratio (a) without and (b) with gating (100 ns). The telescope is located at the point of 0 m viewing the FOV of 50 deg and the laser at that of 100 m. Following parameters are assumed in this calculation; laser power: 100 μJ/pulse, repetition rate: 3000 Hz, exposure time: 1 s.

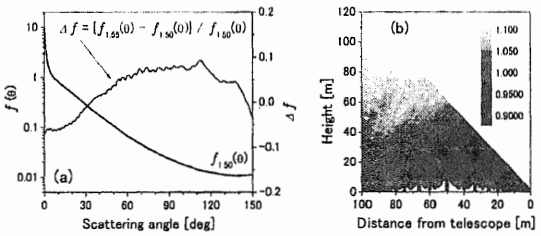

Fig.5 (a) Phase function assumed in the simulation data calculation, and difference between the one and that in the inversion. (b) Error distribution of the extinction coefficient.

3.2 Error estimation of retrieved extinction coefficient

In the inversion of lidar data, an assumption of a phase function is indispensable. The error arising from this assumption is evaluated using a simulation study. The simulation data is calculated as in the previous section. The phase function is obtained from the Mie scattering calculation with the urban model size distribution reported by Jaenicke[10] and the complex refractive index of $1.50 - 0.001i$. The inversion is conducted assuming a different phase function, i.e. the same size distribution but for different values of the complex refractive index, e.g. $1.55 - 0.001i$. These functions are shown in Fig.5(a). The distribution of the inversion error is obtained by comparing the assumed and the retrieved distributions of the extinction coefficient. Figure 5 (b) indicates that the resulting error is within a $\pm 10\%$ range.

4. Bistatic lidar measurement

The preliminary experiment of the bistatic lidar measurement has been conducted using a cooled CCD camera and a pulsed Nd:YAG laser (532 nm). Since the acceptance angel and the baseline distance are both insufficient, the experimental situation is rather limited as compared with the Ashra telescope case. Nevertheless, the two-dimensional measurement reveals the variation of the phase function (mostly from the Rayleigh signal) as expected from the theoretical consideration. The details will be discussed in the presentation at the conference.

Acknowledgment

The financial support from the Frontier Program of the Japan Promotion of Science and Technology Fund is gratefully acknowledged.

References

1. M. Sasaki, A. Kusaka, Y. Asaoka, Design of UHECR telescope with 1 arcmin resolution and 50° field of view, *Nucl. Instr. Meth. Phys. Res.* A492, 49-56 (2002).
2. M. Sasaki, Y. Asaoka, and M. Jobashi, "Self-triggered image intensifier tube for high-resolution UHECR imaging detector," *Nucl. Instr. Meth.* A501, 359-366 (2003).
3. Y. Arai, Y. Aita, T. Aoki, Y. Asaoka, et al. (co-authors: 33), "ASHRA Trigger and Readout Pixel Sensors," Proc. 28th International Cosmic Ray Conference (Tsukuba), 961 (2003).
4. Y. Aita, T. Aoki, Y. Arai, Y. Asaoka, et al. (co-authors: 33), "The ASHRA Detector," Proc. 28th International Cosmic Ray Conference (Tsukuba), 1061 (2003).
5. H. Kuze, S. Fukagawa, N. Takeuchi, Y. Asaoka, and M. Sasaki, "Development of a wide-area imaging lidar for atmospheric monitoring," 29th SICE Remote Sensing Symposium (Tsukuba), 61-64 (2003).
6. K. Meki, K. Yamaguchi, X. Li, Y. Saito, T.D. Kawahara, and A. Nomura, "Range- resolved bistatic imaging lidar for the measurement of the lower atmosphere," *Opt. Lett.* 21 (17), 1318-1320 (1996).
7. J.E. Barnes, S. Bronner, R. Beck, and N.C. Parikh, "Boundary layer scattering measurements with a charge-coupled device camera lidar," *Appl. Opt.* 42 (15), 2647-2652 (2003).
8. C.P. Jacovides, F. Timbios, D.N. Asimakopoulos, and M.D. Steven, "Urban aerosol and clear skies spectra for global and diffuse photosynthetically active radiation," *Agric. For. Meteorol.* 87, 91-104 (1997).
9. Y. Sasano, "Tropospheric aerosol extinction coefficient profiles derived from scanning lidar measurement over Tsukuba, Japan, from 1990 to 1993, *Appl. Opt.*," 35 (24), 4941-4952 (1996).
10. R. Jaenicke, Tropospheric Aerosols, in "Aerosol-Cloud-Climate Interactions" (P.V. Hobbs, ed.), Academic, 1-31 (1993).